Flavonoids in *Ampelopsis grossedentata* as covalent inhibitors of SARS-CoV-2 3CL^pro: Inhibition potentials, covalent binding sites and inhibitory mechanisms

Yuan Xiong [a,b,1], Guang-Hao Zhu [a,1], Ya-Ni Zhang [a], Qing Hu [a], Hao-Nan Wang [a], Hao-Nan Yu [a], Xiao-Ya Qin [b], Xiao-Qing Guan [a], Yan-Wei Xiang [c], Hui Tang [b,*], Guang-Bo Ge [a,*]

[a] *Shanghai Frontiers Science Center for Chinese Medicine Chemical Biology, Institute of Interdisciplinary Integrative Medicine Research, Shanghai University of Traditional Chinese Medicine, Shanghai, China*
[b] *Key Laboratory of Xinjiang Phytomedicine Resource and Utilization, Ministry of Education, Pharmacy School of Shihezi University, Xinjiang, China*
[c] *School of Rehabilitation Science, Shanghai University of Traditional Chinese Medicine, Shanghai 201203, China*

ARTICLE INFO

ABSTRACT

Coronavirus 3C-like protease (3CL^pro) is a crucial target for treating coronavirus diseases including COVID-19. Our preliminary screening showed that *Ampelopsis grossedentata* extract (AGE) displayed potent SARS-CoV-2-3CL^pro inhibitory activity, but the key constituents with SARS-CoV-2-3CL^pro inhibitory effect and their mechanisms were unrevealed. Herein, a practical strategy *via* integrating bioactivity-guided fractionation and purification, mass spectrometry-based peptide profiling and time-dependent biochemical assay, was applied to identify the crucial constituents in AGE and to uncover their inhibitory mechanisms. The results demonstrated that the flavonoid-rich fractions (10-17.5 min) displayed strong SARS-CoV-2-3CL^pro inhibitory activities, while the constituents in these fractions were isolated and their SARS-CoV-2-3CL^pro inhibitory activities were investigated. Among all isolated flavonoids, dihydromyricetin, isodihydromyricetin and myricetin strongly inhibited SARS-CoV-2 3CL^pro in a time-dependent manner. Further investigations demonstrated that myricetin could covalently bind on SARS-CoV-2 3CL^pro at Cys300 and Cys44, while dihydromyricetin and isodihydromyricetin covalently bound at Cys300. Covalent docking coupling with molecular dynamics simulations showed the detailed interactions between the orthoquinone form of myricetin and two covalent binding sites (surrounding Cys300 and Cys44) of SARS-CoV-2 3CL^pro. Collectively, the flavonoids in AGE strongly and time-dependently inhibit SARS-CoV-2 3CL^pro, while the newly identified SARS-CoV-2 3CL^pro inhibitors in AGE offer promising lead compounds for developing novel antiviral agents.

1. Introduction

Over the last two decades, the growing occurrences of coronaviruses-related diseases with high mortality have been one of the long-standing and life-threatening issues to the global population [1]. Currently, the newly emerging coronavirus disease 2019 (COVID-19), a globally infectious disease caused by severe acute respiratory syndrome coronavirus 2 (SARS-CoV-2), has brought a colossal threat to public health, economic development and society safety [2,3]. In the past one-year, exhaustive efforts have been made by the scientists to discover efficacious therapeutics for treating COVID-19, *via* targeting on several validated therapeutic targets. Among all identified therapeutic targets for

combating COVID-19, the chymotrypsin-like protease (3CL[pro]) has drawn great concerns and has been recognized as a pivotal therapeutic target for fighting this pandemic, due to its high conservative and indispensable role in viral replication [4–6]. It has been validated that strong inhibition or dysfunction of 3CL[pro] can successfully block SARS-CoV-2 replication, and further generate benefits in the treatment of COVID-19 [7].

Although a variety of SARS-CoV-2 3CL[pro] inhibitors have been identified recently, the majority of them were restricted to the reversible interactions with the target protease [8–10]. By contrast, the covalent inhibitors could significantly attenuate the proteolytic activity of SARS-CoV-2 3CL[pro] *via* forming a stable chemical bond, which then inactivated this key protease and blocked coronavirus replication. Generally, the covalent inhibitors of target hydrolases bear at least one electrophilic group (such as quinones [11], Michael receptors [12], or some metal elements [13]) that could covalently bind to the nucleophilic residues (such as cysteine). The covalent inhibitors possessed several inherent advantages (such as high specificity, good inhibition potency, and durable interactions) [14], which could bring benefits to both anti-COVID-19 and other CoVs-related diseases. Unfortunately, the promising warheads and lead compounds for the development of efficacious SARS-CoV-2 3CL[pro] covalent inhibitors for treating COVID-19 are rarely reported. Recently, to find more efficacious SARS-CoV-2 3CL[pro] inhibitors with good safety profile, a high-throughput screening campaign was implemented to screen the herbal products with strong SARS-CoV-2 3CL[pro] inhibition activities, by using a fluorescence-based biochemical assay [15,16]. After a large-scale screening of herbal products, we noticed that *Ampelopsis grossedentata* extract (AGE) strongly inhibited SARS-CoV-2 3CL[pro] in both time- and dose-dependently inhibition manners, with the apparent IC_{50} value of 3.44 μg/mL after 60-min preincubation. This finding suggests that AGE should contain the naturally occurring covalent inhibitors of SARS-CoV-2 3CL[pro].

Herein, a practical strategy *via* integrating bioactivity-guided fractionation and purification, mass spectrometry-based peptide identification and time-dependent inhibition assays, was utilized to recognize and characterize the key constituents in AGE with SARS-CoV-2-3CL[pro] inhibitory activities. The results clearly showed that the flavonoid-rich fractions (10–17.5 min on reverse phase liquid chromatography) displayed strong inhibitory activities against SARS-CoV-2-3CL[pro]. After then, the major constituents in these bioactive factions were isolated and their structures as well as inhibitory effects on SARS-CoV-2-3CL[pro] were carefully identified. Among all isolated constituents, dihydromyricetin, isodihydromyricetin and myricetin strongly inhibited SARS-CoV-2-3CL[pro] in dose- and time- dependent manners. On the basis of the chemical structures of these newly identified SARS-CoV-2-3CL[pro] inhibitors, we postulated their catecholic groups in B-ring were easily oxidized into orthoquinones, which in turn, covalently modifying SARS-CoV-2-3CL[pro] (Fig. S4). In these cases, further mass spectrometry-based peptide assays coupling with molecular dynamics simulations were carried out to reveal the covalent binding sites and to explore the inhibitory mechanisms of these naturally occurring flavonoids.

2. Materials and methods

2.1. Chemicals and reagents

The Smt3-SARS-CoV-2 3CL[pro] codon was cloned into the pET29a (+) vectors by GENEWIZ, Inc. (Beijing, China). *Escherichia coli* (*E. coli*) BL21 (DE3) was gained from Shanghai Weidi Biotechnology Co., Ltd. (Shanghai, China). Tris-Base was obtained from Amresco (USA). Ethylene Diamine Tetraacetic Acid (EDTA) was gained from Dalian Meilun Biotechnology Co. Ltd. (Dalian, China). Lysozyme, sodium chloride (NaCl), imidazole, dithiothreitol (DTT), phenylmethylsulfonyl fluoride (PMSF), and hydrochloric acid (HCl), were purchased from Sinopharm Chemical Reagent Co., Ltd. (Shanghai, China). 2-[4-(2-hydroxyethyl) piperazin-1-yl] ethane sulfonic acid (HEPES),

NH₄HCO₃, urea, iodoacetamide (IAA), chymotrypsin and trypsin were provided by Sigma-Aldrich (St. Louis, MO, USA). Super Nuclease was purchased from Sino Biological Inc. (Beijing, China). One hundred and two herbal products were provided by Tianjiang Pharmaceutical Co., Ltd. (Jiangsu, China), two standard extracts (*St. John's Wort* and *Ginkgo Folium*) were bought from Baoji Guokang Bio-Technology Co.,Ltd and Hubei Nokete Pharmaceutical Co.,Ltd,. *Ampelopsis grossedentata* extract was attained from Eastsign Foods Co., Ltd. (Quzhou, China). The reported covalent inhibitor of SARS-CoV-2 3CL[pro] (ebselen) was provided by TCI (Shanghai, China) [17]. Fluorescent substrate (Dabcyl-KNSTLQSGLRKE-Edans) was purchased from Shanghai Sangon Biological Engineering & Technology and Service Co. Ltd. (Shanghai, China), with the purity of 99%. The stock solution of this fluorescent substrate was prepared by Millipore water and stored at 4 °C. HPLC grade methanol, acetonitrile, dimethyl sulfoxide (DMSO) and formic acid were all ordered from Tedia (Fairfield, USA). DMSO-d_6 and MeOD were provided by Adamas-beta (Shanghai, China) for ¹H and ¹³C NMR analyses. Millipore water (Millipore, Bedford, USA) was used for preparing PBS buffer (pH 7.4, 100 mM) that was stored at 4 °C until use.

2.2. SARS-CoV-2 3CL[pro] inhibition assay

A fluorescence-based enzyme inhibition assay in 96-well plate format was used to assess the SARS-CoV-2 3CL[pro] inhibition activity [15,16]. The hydrolytic rates of 3CL[pro]-catalyzed Dabcyl-KNSTLQSGLRKE-Edans were monitored in a reaction mixture (100 μL, total volume) with or without each tested inhibitor. Briefly, the SARS-CoV-2 3CL[pro] (4 μg/mL, final concentration) was preincubated with analytes / DMSO (as a control group) in PBS (pH 7.4, 100 mM, 1 mM EDTA) at 37 °C for 60 min or 0.5 min. Then the reaction proceeded for 20 min after added the Dabcyl-KNSTLQSGLRKE-Edans (20 μM, final concentration). The generated fluorescent signals (excitation/emission, 340 nm/490 nm) were continuously monitored by the microplate reader (SpectraMax® iD5, Molecular Devices, Austria).

2.3. Bioactivity-guided fractionation of AGE

A bioactivity-guided fractionation strategy was applied to quickly find out the bioactive fractions in AGE, which was supported by one Shimadzu UFLC system (Kyoto, Japan) equipped with an SPD-M 30A PDA detector. Water-0.1% formic acid (A) and acetonitrile (B) were optimized as the mobile phases in gradient conditions: 0.01–2 min, 95% A; 15–20 min,70%–25% A; 22–25 min, 95% A. The AGE sample (5 μL, 10 mg/mL) was injected and separated on a Shim-pack VP-ODS C18 column (2.0 × 250 mm, 4.6 μm) with the flow rate of 0.4 mL/min at 40 °C, and the LC fractions were collected every 2.5 min. Ten collected LC fractions were dried under vacuum pressure, and then redissolved in DMSO for assessment of 3CL[pro] inhibition activity.

2.4. Isolation and identification of the major bioactive constituents in AGE

An LC-TOF-MS/MS system (Foster City, CA, USA) equipped with a Shimadzu UFLC system (Kyoto, Japan) was used to identify the major constituents in the bioactive fractions (10–17.5 min) of AGE in both positive and negative ion modes. The mass parameters were listed in Table S1. Meanwhile, five major constituents were isolated by using a preparative HPLC (Waters, USA). The AGE sample (10 mL, 10 mg/mL) was continuously injected and separated on a Acchrom-C18 column (50 × 450 mm, 7 μm), accompanied by 80% of water-0.1% formic acid and 20% of acetonitrile: methanol (4:1) with the flow rate of 65 mL/min. Five isolated constituents in AGE were enriched and dried *in vacuo* separately, the solid of each constituent was collected for structural characterization and SARS-CoV-2 3CL[pro] inhibition assay.

2.5. Identification of the covalent binding sites of three flavonoids on SARS-CoV-2 3CL^{pro}

To identify the covalently modified sites for three flavonoids on SARS-CoV-2 3CL^{pro}, the peptides of target enzyme co-incubated with or without each tested flavonoid were analyzed by using a nanoLC-MS/MS system [17,18–20]. Firstly, the SARS-CoV-2 3CL^{pro} (147 μg, total content) was co-incubated with inhibitors (400 μM, final concentration) at 37 °C overnight. After that, the urea (6 M, final concentration) was added into the mixtures at 75 °C to denature SARS-CoV-2-3CL^{pro}. In order to complete the alkylation of protein, the modified-SARS-CoV-2-3CL^{pro} were separately co-incubated with DTT (1 mM, final concentration) for 10 min at 95 °C, and then treated with IAA (3 mM, final concentration) at 30 °C for 30 min in the dark. The protein precipitations were collected after added ice-cold acetonitrile and centrifugated at 16000 g for 10 min, which further dried in a termovap sample concentrator (ATR, AutoVap S60, USA). After then, the enriched proteins were redissolved in NH$_4$HCO$_3$ solution (pH 8.0, 50 mM), digested by chymotrypsin and trypsin (the content of protein: SARS-CoV-2 3CL^{pro} ratios were 1:40), respectively. The produced peptides were desalted on a MonoSpin C18 column (GL Sciences Inc.), the eluents were dried *in vacuo* and resolved in 0.1% formic acid for analyses.

The samples (contained 0.5–1 μg peptides) were injected into nanoLC system (EASY-nLC 1200, Thermo Fisher Scientific, USA), separated at a self-packed analytical C18 column (20 μm × 360 μm × 200 mm, 3 μm) with the flow-rate of 0.3 μL/min. Water containing 0.1% formic acid (A) and 80% acetonitrile-20% water (B) were used as the mobile phases, the elution conditions were as follow: 0–1 min, 1%–6% B; 1–47 min, 6%–35% B; 47–54 min, 35%–37% B; 54–56 min, 37%–95% B; 56–65 min, 95% B. The full MS data were recorded by using the data-dependent mode on the Hybrid Quadrupole-Orbitrap mass spectrometer (Q Exactive™ HF-X, Thermo Fisher Scientific, USA) from m/z 300–m/z 1800, with the resolution of 60,000 (AGC target 3e6, maximum IT 50 ms). The analytes were fragmented in the HCD (Higher Energy Collision Dissociation) mode with resolution of 15,000 at a 28% normalized collision energy (AGC target 1e5, maximum IT 30 ms).

2.6. Inactivation kinetic analysis for three flavonoids on SARS-CoV-2 3CL^{pro}

The inactivation kinetics for three flavonoids were investigated as the reported procedure [21]. Firstly, two incubation mixture groups (group A and group B) were prepared for use. Group A (90 μL) were comprised of Dabcyl-KNSTLQSGLRKE-Edans (20 μM, final concentration) and PBS (pH 7.4, 100 mM, 1 mM EDTA). Group B (100 μL) contained flavonoid and SARS-CoV-2 3CL^{pro} that were co-incubated at 37 °C in tubes filled with PBS (pH 7.4, 100 mM, 1 mM EDTA). Then the mixtures (10 μL) in group B were transferred to group A at different preincubation time to initiate the hydrolytic reaction. After incubation for another 20 min at 37 °C, the hydrolytic reaction was quenched by adding ice-cold acetonitrile (100 μL). The natural logarithm of the residual SARS-CoV-2 3CL^{pro} activity was plotted against the preincubation time.

2.7. Covalent docking and molecular dynamics simulations

The covalent docking was carried out through the covalent docking module of MOE (Molecular Operating Environment 2019.01, Chemical Computing Group Inc., Montreal, Canada). Firstly, the crystal structure of SARS-CoV-2 3CL^{pro} (PDB Code: 6XHU, [22]) was download for preliminary treatment by using the QuickPrep module, including adding hydrogens and partial charges, optimizing the hydrogen bond network and minimizing energies. Then, the orthoquinone form of myricetin (QFM) was constructed and minimized energy in the Builder panel. Next, the covalent reaction formula for QFM and cysteine residuals was generated by MarvinSketch and imported to MOE for covalent docking

module. Finally, with the help of GBVI/WSA dG, these generated conformations of the rigid receptor were refined and estimated the binding scores [23]. The pose with the lowest S score was selected as the initial conformation of QFM-3CL^{pro} complexes.

To perform the molecular dynamics (MD) simulations for QFM-3CL^{pro} complexes, it was necessary to get the force field of non-standard amino acid (Cys-QFM), which was generated by AmberTools20 (AMBER 2020, University of California, San Francisco, USA). The detailed procedures were as follows. At first, AM1-BCC charges of the Cys-QFM complex were calculated [24]. Then, atoms, bonds, angles, and dihedral parameters of Cys-QFM complex were established *via* atom types of amber99sb-ildn force field and checked by parmchk2 [25]. Next, coordinate and topology files of Cys-QFM complex were created by leap program, and then translated to the GROMACS topology file *via* ACYPE [26,27]. Finally, manually written residue topology parameter file (rtp file) as per the GROMACS topology file and manually written hydrogen database file (hdb file) were loaded into the libraries files of amber99sb-ildn force field.

Systems of QFM-3CL^{pro} complexes were established for simulations. Prior to MD simulations, an energy minimization of 50,000 steps steepest descent was performed. To neutralize the charges of the protein-solvent system, SARS-CoV-2 3CL^{pro} and QFM-3CL^{pro} complexes were separately solvated with the TIP3P water model including sodium ions. Then, the system was equilibrated, including 100 ps for NVT heating to 310 K, and 100 ps for NPT. Finally, the system was subjected to 50 ns MD at 310 K (V-rescale thermostat) under a pressure of 1 bar (Parrinello–Rahman barostat). To analyze the interactions of QFM-3CL^{pro} complexes, we clustered the equilibrium conformations [28], and the largest center structure was selected to study the interactions by creating its stereoscopic picture *via* Discovery Studio Visualizer (BIOVIA Discovery Studio 2019, Dassault Systèmes, San Diego, USA).

2.8. Statistical analysis

IC$_{50}$ and K_I values were evaluated by nonlinear regression using Graph Pad Prism 7.0 software (GraphPad Software, Inc., La Jolla, USA). The nanoLC-MS/MS data was searched by Protein Discovery 2.4 (Thermo Scientific) by using the Sequest HT algorithm for peptide identification.

3. Results

3.1. Inhibition of SARS-CoV-2 3CL^{pro} by herbal products

Firstly, the inhibitory potentials of 105 herbal extracts (100 μg/mL, final concentration) on SARS-CoV-2 3CL^{pro} were assayed by using Dabcyl-KNSTLQSGLRKE-Edans as the fluorescent substrate. From the preliminary screening, AGE exhibited the most potent SARS-CoV-2 3CL^{pro} inhibition activity (Fig. 1). The residual activity of SARS-CoV-2 3CL^{pro} in the presence of AGE (100 μg/mL, final concentration) was 0.26%. As depicted in Fig. 2, AGE could dose-dependently inhibit SARS-CoV-2 3CL^{pro}-catalyzed Dabcyl-KNSTLQSGLRKE-Edans cleavage reaction, with IC$_{50}$ value of 3.44 μg/mL. Meanwhile, time-dependent inhibition assays showed that AGE time-dependently inhibited SARS-CoV-2 3CL^{pro}, with an obvious shift in apparent IC$_{50}$ value (the ratio of IC$_{50}$ = 3.63) when AGE was pre-incubated with SARS-CoV-2 3CL^{pro} at various preincubation times. These findings demonstrate that AGE strongly inhibits SARS-CoV-2 3CL^{pro} in dose- and time- dependent manners, implying that some natural constituents in AGE may covalently bind with SARS-CoV-2 3CL^{pro}.

3.2. Identification of the naturally occurring SARS-CoV-2 3CL^{pro} inhibitors in AGE

Then, a practical strategy *via* integrating bioactivity-guided fractionation and purification, as well as inhibition assay, was used to
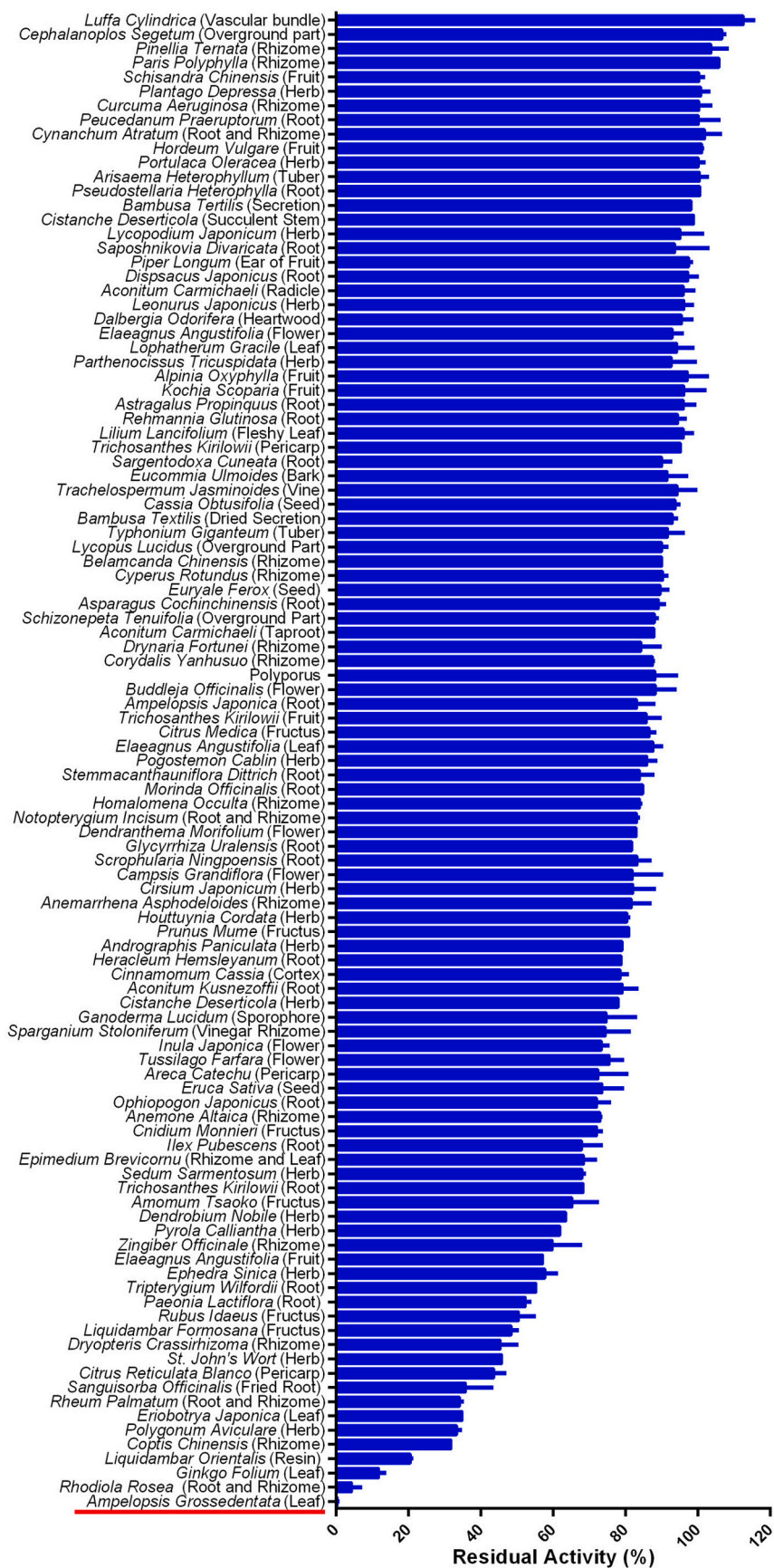
Fig. 1. The inhibitory effects of 105 herbal products (100 μg/mL, final concentration) against SARS-CoV-2 3CL^{pro}.
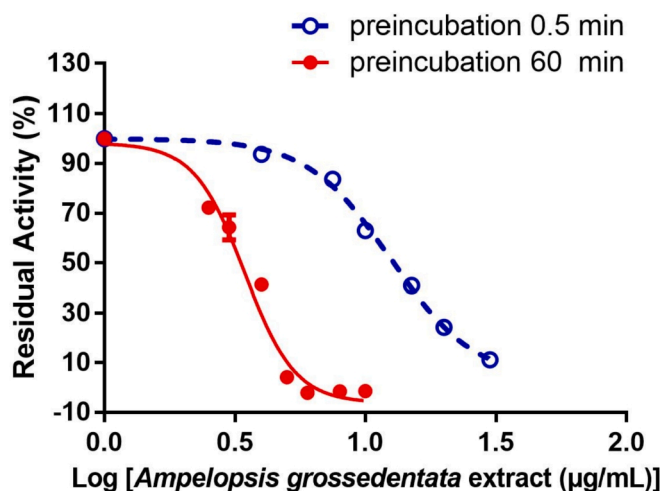
Fig. 2. The dose-inhibition curves of 0.5 min and 60 min of AGE against SARS-CoV-2 3CL^pro.

identify the key constituents in AGE. From the results exhibited in Fig. 3, within ten fractions, F5, F6 and F7 possessed strong inhibitory properties against SARS-CoV-2 3CL^pro. After then, five major peaks of the bioactive fractions (10–17.5 min) were isolated, while their structures and effects of inhibiting SARS-CoV-2-3CL^pro were characterized. The MS^1 and MS^2 spectra of these natural compounds were shown in Table 1, Figs. S6–S10, while their ^{1}H and ^{13}C NMR spectra were presented in Figs. S19–S23. These spectra data clearly suggested that five major constituents in the bioactive fractions of AGE (10–17.5 min) were five flavonoids, including dihydromyricetin, isodihydromyricetin, myricitrin, taxifolin and myricetin.

After then, the inhibition potentials of five isolated flavonoids against SARS-CoV-2 3CL^pro were assayed by using three different doses. As depicted in Fig. 4, the results presented that dihydromyricetin, iso-dihydromyricetin, as well as myricetin showed strong inhibition effects against SARS-CoV-2-3CL^pro (IC$_{50}$ < 5 μM). Meanwhile, taxifolin and myricitrin moderately inhibited SARS-CoV-2 3CL^pro, with the IC$_{50}$ values ranging from 10 μM to 100 μM. The dose-response curves of five flavonoids in AGE bioactive fractions (10–17.5 min) against SARS-CoV-2 3CL^pro were also plotted by using increasing concentrations of each flavonoid (Fig. 5, Fig. S12). As listed in Table 2, dihydromyricetin, iso-dihydromyricetin and myricetin could strongly inhibit SARS-CoV-2 3CL^pro, with IC$_{50}$ values of 4.91 μM, 3.73 μM and 1.21 μM after 60-min preincubation, respectively. Notably, the inhibitory activity of myricetin was superior to the reported positive inhibitor ebselen (Fig. S11, a newly reported covalent inhibitor of SARS-CoV-2 3CL^pro, IC$_{50}$ = 2.62 μM).

Meanwhile, time-dependent inhibition assessments for these five flavonoids were also carried out. The results clearly demonstrated that the inhibition potency of dihydromyricetin, isodihydromyricetin, myricitrin and myricetin against SARS-CoV-2 3CL^pro would be enhanced with the pre-incubation time, with the IC$_{50}$ ratios to be 7.05-fold, 7.78-fold, 8.32-fold, and 17.72-fold, respectively (Table 2, Fig. 5). These findings suggest that dihydromyricetin, isodihydromyricetin, myricitrin and myricetin are the key bioactive constituents in AGE that can dose- and time- dependently inhibit SARS-CoV-2 3CL^pro.

3.3. Identification of the covalent binding sites of three flavonoids on SARS-CoV-2 3CL^pro

Next, the covalent binding sites of dihydromyricetin, iso-dihydromyricetin and myricetin on SARS-CoV-2 3CL^pro were identified by using mass spectrometry. From the view of chemical structures of these naturally occurring flavonoids, all these compounds bear a
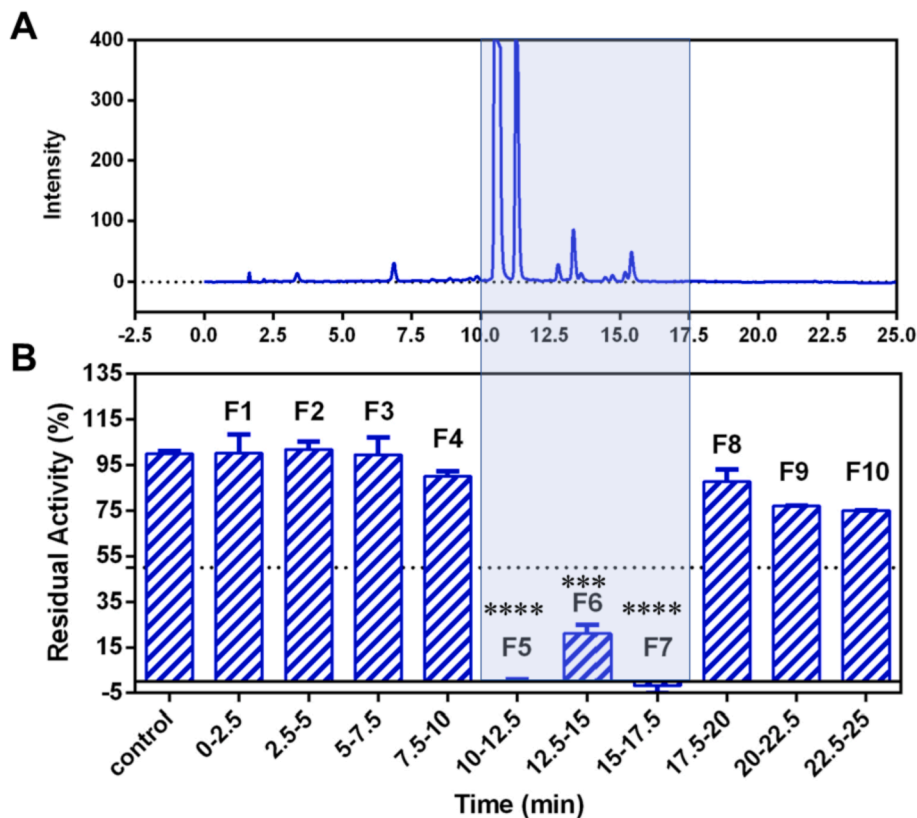

Fig. 3. Fingerprinting analysis of AGE by LC-UV in 290 nm (A), and the SARS-CoV-2 3CL^pro inhibition profiles of the LC fractions collected at 2.5 min intervals (B). (***p < 0.001, ****p < 0.0001, compared with the control group).

Table 1

Identification and characterization of five major constitutes in the bioactive fractions of AGE by LC-PDA-TOF-MS/MS.

No.	t_R (min)	λ_{max} (nm)	Ionization	*m/z*	Formula	Fragment ions	Identification
1	10.611	290	[M-H]⁻	319.0469	$C_{15}H_{12}O_8$	319.0469,301.0354, 283.0262, 257.0461,215.0352,193.0143,175.0035, 125.0245	Dihydromyricetin
2	11.413	293	[M-H]⁻	319.0462	$C_{15}H_{12}O_8$	319.0462,301.0370, 257.0464, 215.0358, 193.0149, 175.0047, 125.0252	Isodihydromyricetin
3	12.894	352	[M-H]⁻	463.0902	$C_{21}H_{20}O_{12}$	463.0902, 317.0330, 316.0245, 217.0263, 270.0187	Myricitrin
4	13.464	289	[M-H]⁻	303.0515	$C_{15}H_{12}O_7$	303.05-15, 275.0565, 241.0517, 217.0520, 125.0251	Taxifolin
5	15.521	370	[M-H]⁻	317.0310	$C_{15}H_{10}O_8$	317.0310, 289.0360, 271.0260, 178.9990	Myricetin
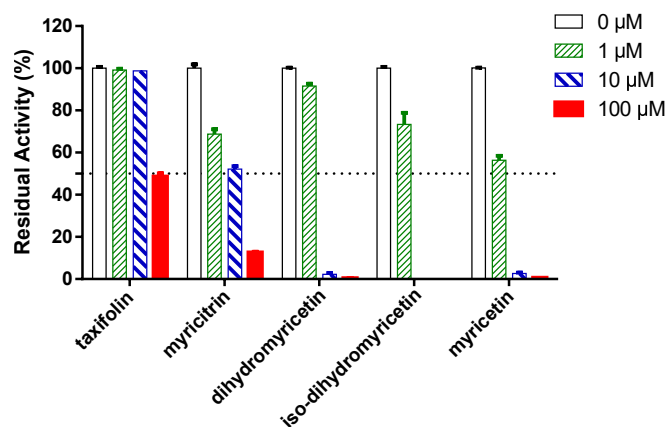
Fig. 4. Inhibitory effects of five major constituents in the bioactive fractions from AGE against SARS-CoV-2 3CL^pro.

catecholic group at the B-ring, which can be easily oxidized to form orthoquinones that can covalently bind on the biothiols or the cysteines in target proteins (Fig. 6) [28,29]. In this case, the generated MS/MS spectra were analyzed by searching covalent modifications on cysteines of SARS-CoV-2 3CL^pro, with the molecular mass increments of 316.24 Da (myricetin) and 318.25 Da (dihydromyricetin or isodihydromyricetin).

As shown in Table 3, following co-incubation of SARS-CoV-2 3CL^pro with each tested flavonoid, several cysteine residues in the peptides of SARS-CoV-2 3CL^pro could be modified by the orthoquinone forms of these three flavonoids. From Fig. 7, Fig. S14, Fig. S15, all tested flavonoids (myricetin, dihydromyricetin and isodihydromyricetin) could covalently modify Cys300, a key residue located at domain III (residuals 198-303) of SARS-CoV-2 3CL^pro (Fig. S13). Several reports state that domain III (especially ²⁹⁰E-V³⁰³) functions as a crucial part to maintain the dimer conformation of active 3CL^pro, mutation or modification of the key residuals (such as Gln290, Arg298 and Gln299) would result in the instability or inactivation of this key enzyme [30–33]. Thus, it was easily conceivable that the surrounding micro-environment or the pivotal interactions for the formation of the dimer of active SARS-CoV-2 3CL^pro might be changed or destroyed *via* modification of Cys300 by these naturally occurring flavonoids.

In addition to Cys300, myricetin can also covalently bind on Cys44, which is near the catalytic site of SARS-CoV-2 3CL^pro (Fig. 7, Fig. S13). Recently study has found that Cys44 is a hyper-reactive cysteine with higher nucleophilicity than Cys145, which is recognized as a promising binding site for designing and developing covalent inhibitors of this key enzyme [34]. The covalent binding of myricetin on Cys44 might block 3CL^pro-catalyzed peptide-cleavage reactions. These findings suggest that myricetin and its analogous in AGE can covalently bind on some key
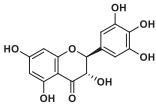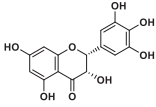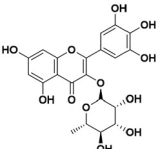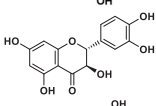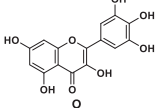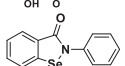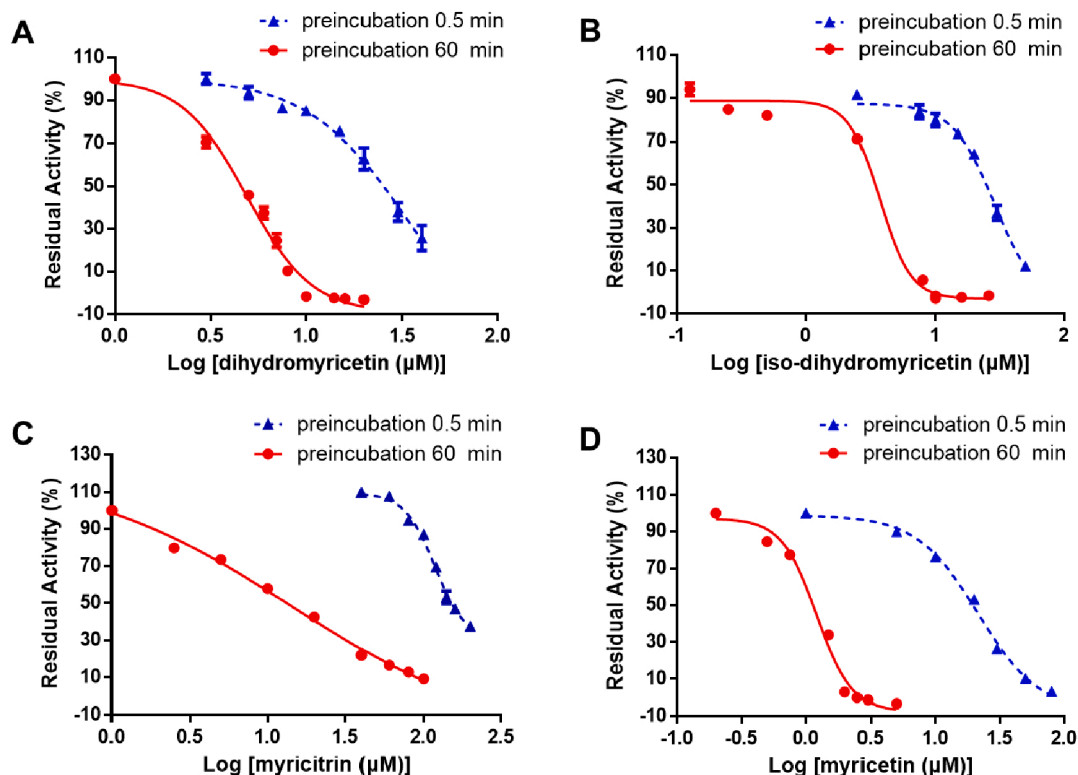

Fig. 5. Dose- and time- dependent inhibition curves of dihydromyricetin (A), isodihydromyricetin (B), myricitrin (C) and myricetin (D) against SARS-CoV-2 3CL^pro.

Table 2
The inhibition parameters of the bioactive constituents in AGE against SARS-CoV-2 3CL^{pro}.

No.	Compound	Structure	IC$_{50}$ (μM)		Ratio	K_I (μM)	K_{inact} (min^{-1})
			0.5 (min)	60 (min)			
1	Dihydromyricetin		34.61	4.91	7.05	67.35	0.064
2	Isodihydromyricetin		29.04	3.73	7.78	62.43	0.058
3	Myricitrin		118.10	14.22	8.32	–	–
4	Taxifolin		>200	72.72	>2.75	–	–
5	Myricetin		21.44	1.21	17.72	6.33	0.013
6	Ebselen[a]		3.11	2.62	1.18	–	–

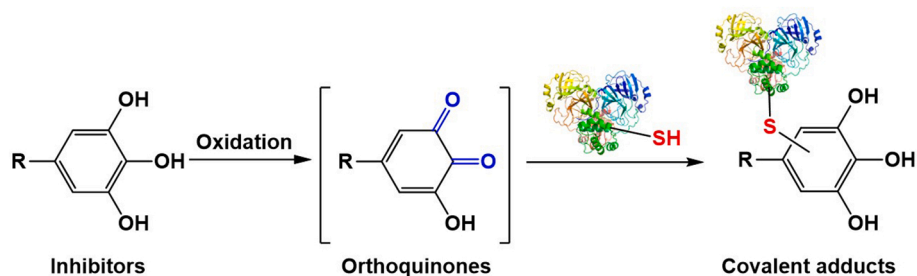[a] A known positive covalent inhibitor for SARS-CoV-2 3CL^{pro}.

Fig. 6. The proposed scheme of the newly identified flavonoid-type inhibitors covalently bind on the biothiols of SARS-CoV-2 3CL^{pro}.

Table 3
Identification of the covalent binding sites for three flavonoids on SARS-CoV-2 3CL^{pro} by nanoLC-MS/MS.

Inhibitor	Peptide	Modifications	Charge	m/z (Da)	MH$^+$ (Da)	MH$^+$ (Da) (Theoretical)	Mass accuracy ΔMr (ppm)	t_R(min)
Dihydromyricetin	[295]DVVRQ**C***SGVTF[305]	Cys300	2	764.8166	1528.6260	1528.6260	−0.04	41.157
Isodihydromyricetin	[295]DVVRQ**C***SGVTF[305]	Cys300	2	764.8170	1528.6267	1528.6260	0.43	41.743
Myricetin	[41]HVI**C***TSEDMLNPNYEDLLIR[60]	Cys44	3	897.7310	2691.1785	2691.1587	7.36	48.006
	[295]DVVRQ**C***SGVTF[305]	Cys300	2	763.8091	1526.6108	1526.6102	0.46	42.820

*The amino acids modified by inhibitors.

cysteines of SARS-CoV-2 3CL^{pro}, while myricetin can concurrently modify both Cys300 and Cys44. Meanwhile, these findings can partially explain the potent inhibition efficacy of myricetin, in comparison with its analogous (such as dihydromyricetin or isodihydromyricetin).

3.4. Inactivation kinetics of three flavonoids on SARS-CoV-2 3CL^{pro}

The inactivation kinetics for three flavonoids were further investigated to evaluate the inactivation potency of these naturally occurring SARS-CoV-2 3CL^{pro} inhibitors. To this end, the inactivation kinetic curves were plotted by using various inhibitor concentrations with increasing pre-incubation times. As shown in Fig. S16 and Fig. 8, dihydromyricetin, isodihydromyricetin and myricetin could inactivate SARS-CoV-2 3CL^{pro} activity *via* dose- and time- dependent manners, their K_I values were determined as 67.35 μM, 62.43 μM and 6.33 μM, respectively, while K_{inact} values were calculated as 0.064 min^{-1}, 0.058 min^{-1} and 0.013 min^{-1}, respectively. These results suggest that three flavonoids are naturally occurring time-dependent SARS-CoV-2 3CL^{pro} inhibitors, while myricetin exhibited the strongest inactivation potency, which encourages us to further investigate the interactional modes of
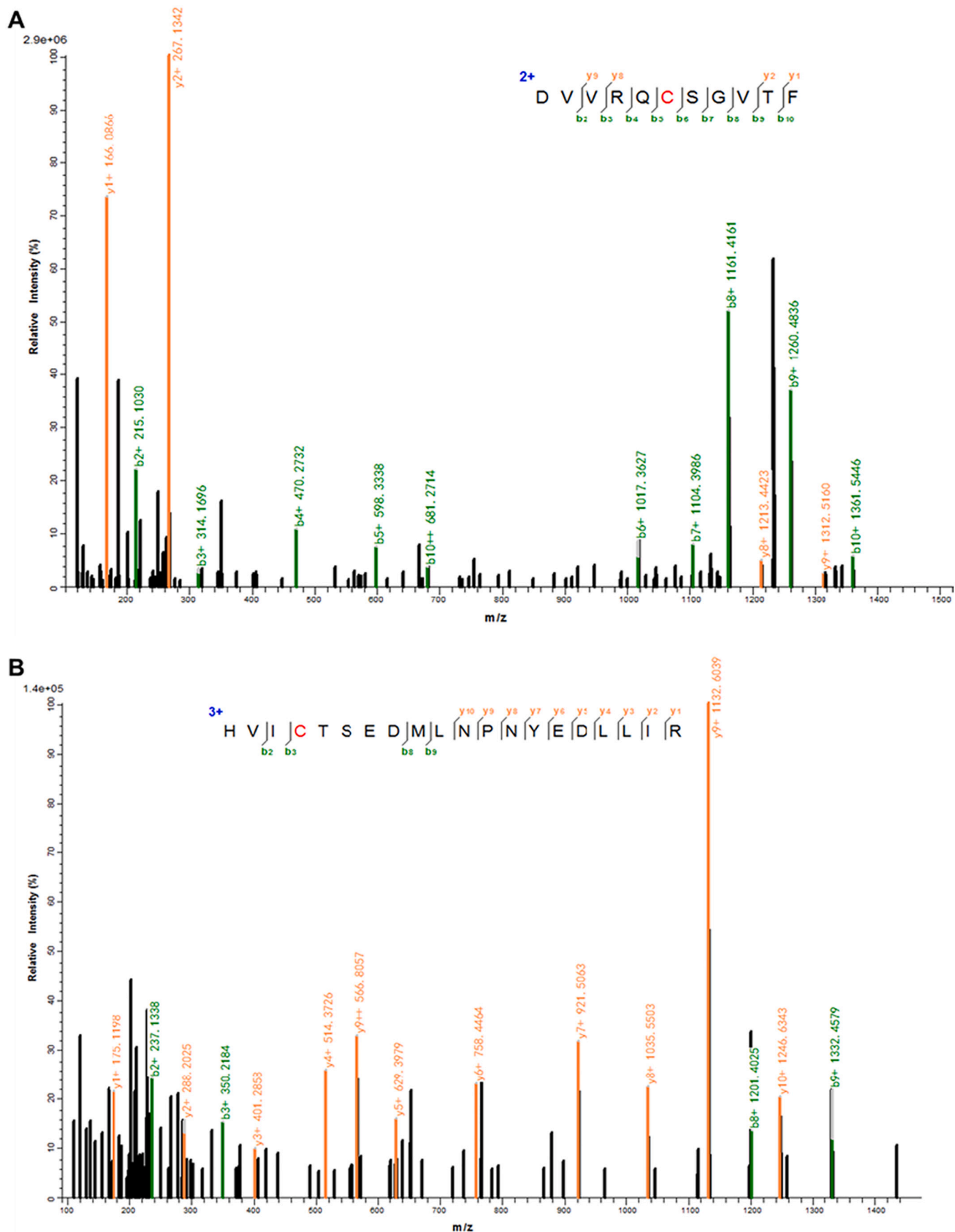
Fig. 7. The MS² spectra of the peptide DVVRQCSGVTF (A) and HVICTSEDMLNPNYEDLLIR (B) covalently modified by myricetin.
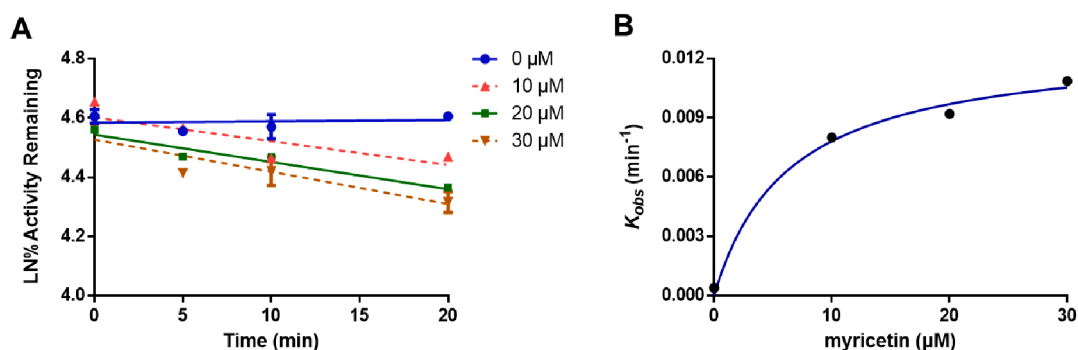
Fig. 8. Time- and concentration-dependent inhibition of myricetin (A) on SARS-CoV-2 3CL^{pro}. The hyperbolic plot of k_{obs} of SARS-CoV-2 3CL^{pro} *vs.* myricetin (B) concentrations.

this agent with SARS-CoV-2 3CL^{pro}.

3.5. Covalent docking and molecular dynamics simulations

Finally, covalent docking simulations and molecular dynamics simulations were carefully conducted for QFM that covalently bound in site 1 (near Cys300) and site 2 (near Cys44) of SARS-CoV-2 3CL^{pro} to explore the key interactions between this agent and the target enzyme. As shown in Fig. 9B and Fig. S17, when QFM covalently bound to the sulfur atom of Cys300, this agent mainly interacted with the surrounding amino acid residuals (including Val296, Val297, Gly2 and Ile213) by hydrogen bonding. As for site 2 (near Cys44), it was observed from Fig. 9D and Fig. S18 that QFM could form an adduct *via* covalently bound on Cys44, while this agent interacted with some residuals in site 2 through

hydrogen bonding (*via* forming a carbon hydrogen bond and conventional hydrogen bonds) and hydrophobic bonding (amide-Pi stacked & Pi-alkyl). These results manifest that the orthoquinone form of myricetin can covalently bind in both site 1 (near Cys300) and site 2 (near Cys44) on SARS-CoV-2 3CL^{pro}, while the covalent modifications at these two sites may lead SARS-CoV-2 3CL^{pro} to its inactive forms.

4. Discussion

Currently, the COVID-19 global pandemic has already brought strong impact on human health, economic growth and social stability. To efficiently fight against COVID-19, the scientists have made great endeavors to develop novel therapeutics *via* targeting the validated therapeutic targets. Among all validated therapeutic targets, 3CL^{pro} has
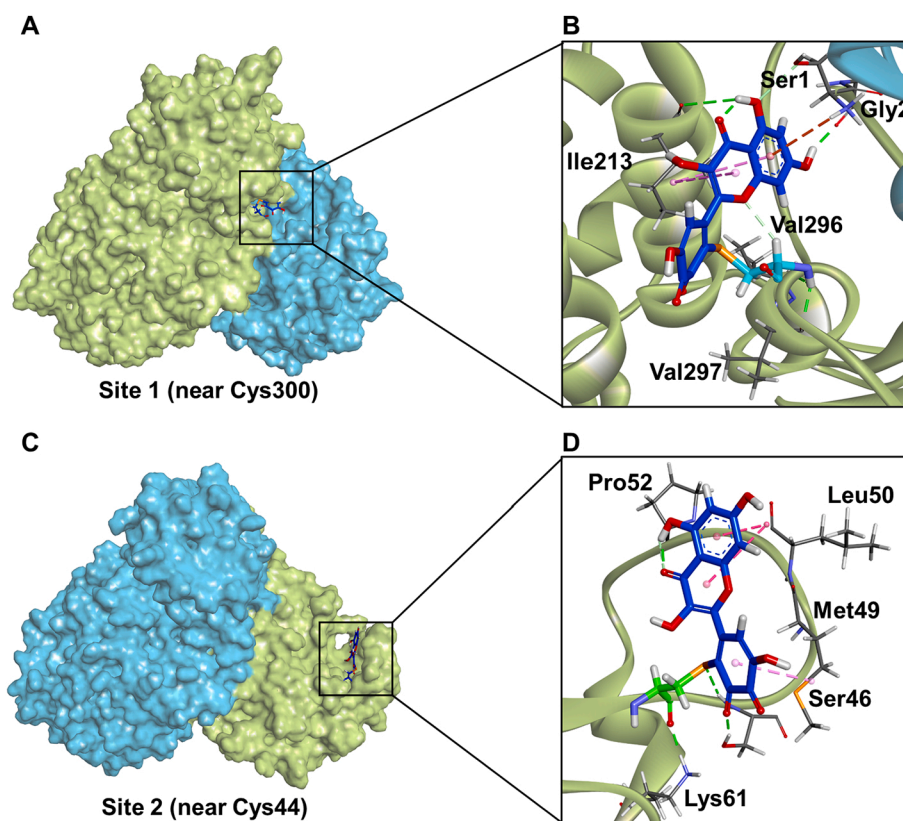

Fig. 9. The stereo view of the crystal structure SARS-CoV-2 3CL^{pro} (PDB Code: 6XHU) that was covalently bound on the orthoquinone form of myricetin at Cys300 (A) or Cys44 (C). The detailed interactions between SARS-CoV-2 3CL^{pro} and the orthoquinone form at Cys300 (B) or Cys44 (D).

been validated as a key target for treating SARS-CoV-2 and other coronavirus, owing to the exceptionally important role of 3CL^pro during the viral life cycle [35]. Over the past one year, a variety of SARS-CoV-2 3CL^pro inhibitors have been found, but only several compounds are identified as the covalent inhibitors of this vital enzyme *via* forming chemically stable and irreversible bonds [13]. Given that the covalent inhibitors always display good inhibition potency in living systems, the covalent inhibitors of 3CL^pro are considered as a good choice to block the SARS-CoV-2 multiplication *via* inactivating the proteolytic activity of 3CL^pro. Thus, it is urgent and highly desirable to find more efficacious SARS-CoV-2 3CL^pro covalent inhibitors with improved safety profiles, which may offer the promising lead compounds for developing novel anti-COVID-19 agents.

In these cases, a high-throughput screening campaign was conducted for discovering effective SARS-CoV-2 3CL^pro covalent inhibitors from herbal products. Among all tested herbal products, AGE demonstrated the most potent SARS-CoV-2 3CL^pro inhibition activity, while this herbal extract inhibited this key enzyme in time- and dose- dependent manners. This finding intrigued us to reveal the key bioactive constituents in AGE that could covalently bind to SARS-CoV-2 3CL^pro. In Southeast China, *Ampelopsis grossedentata* is a flavonoid-rich (w/w > 40%) medicinal herb, whose dried leaves and stems are popularly used as healthy tea to prevent chronic disorders by reducing hypertension, regulating plasma lipids and blood glucose [36–39]. Herein, we identified that three abundant flavonoids (dihydromyricetin, isodihydromyricetin and myricetin) in AGE could strongly inhibit SARS-CoV-2 3CL^pro by covalently binding with two key cysteines on this target enzyme. Previous reports have reported that the flavonoids (myricetin and dihydromyricetin) in AGE exhibit multiple beneficial effects including anti-inflammatory, anti-coagulative, as well as pulmonary fibrosis inhibition activities [34,40–42]. Thus, *Ampelopsis grossedentata* could be used as a healthy plant-based supplement for treating COVID-19, which might relieve the COVID-19-related symptoms in both the respiratory tract system and alimentary system. Moreover, this edible herb can be co-administrated with other antiviral herbs (such as *Scutellaria baicalensis* [43], *Glycyrrhiza uralensis* [44] and *Ephedra sinica* [45]) that contain other anti-SARS-CoV-2 phytochemicals with diverse inhibition mechanisms or various binding targets, in which the combination use may bring additive or synergistic antiviral effects for the treatment of COVID-19.

Notably, three newly identified SARS-CoV-2 3CL^pro covalent inhibitors (dihydromyricetin, isodihydromyricetin and myricetin) in AGE were also found with the inhibition against SARS-CoV helicase [46] and SARS-CoV3CL^pro [47], as well as high affinities with the ACE2 receptor [40], suggesting that these agents hold sufficient potentials to develop as the broad-spectrum anti-coronavirus agents *via* targeting multiple key druggable targets. However, the poor cell-permeability and poor metabolic stability of these natural flavonoids strongly hampered the wide applications of these flavonoids in clinical settings [42]. Therefore, it is necessary to used more practical approaches (such as structural optimizations or drug delivery technologies) to develop more efficacious agents for combating COVID-19 pandemic. Considering that the naturally occurring flavonoids could be extensively metabolized by UDP-glucuronosyltransferases (UGTs) or other conjugative enzymes in humans [48], AGE could be co-administrated with other herbal medicines containing strong inhibitors against human UGTs, such as Fructus Psoraleae [49], or UGTs inhibitors like amentoflavone [50] and licochalcone A [51], which might improve the *in vivo* therapeutic effects of AGE against COVID-19. Furthermore, this study also offered several leading compounds and a key warhead for designing and developing more efficacious SARS-CoV-2 3CL^pro covalent inhibitors. Among all tested flavonoids isolated from AGE, myricetin was identified as the most potent SARS-CoV-2 3CL^pro covalent inhibitor, owing to this agent could concurrently label both Cys300 and Cys44 of this key enzyme. Our findings suggested that the ortho-trihydroxyl group in the B ring of these flavonoids was a crucial pharmacophore for covalently binding on 3CL^pro, as well as SARS-CoV-2-3CL^pro inhibitory activities. Meanwhile,

the plane structures without glycosides were propitious to the process of covalent reactions. In future, this key warhead will be conducive to design a new generation of efficacious anti-COVID-19 medications, while these pyrogallol-containing compounds can be used as practical probes or tools to identify the covalent inhibitors for cysteine proteases. More importantly, compared with the cysteine residuals in SARS-CoV-2 3CL^pro (such as Cys44 and Cys145), Cys300 is suggested as a more desired ligand-binding site for developing covalent inhibitors of SARS-CoV-2 3CL^pro, owing to its unique location at the dimeric surface of SARS-CoV-2 3CL^pro that is more liable to be covalently modified by small molecules. The mutation or molecule-modifications of the conserved Cys300 may destroy the dimerization of 3CL^pro and further cause the active form of this enzyme into an inactive monomer, which provide new insight to design novel agents for combating fatal β-coronavirus, including SARS-CoV and SARS-CoV-2.

5. Conclusion

In summary, this study reported that both AGE and the major constituents or the flavonoid-rich fractions of this herbal extract could strongly inhibit SARS-CoV-2 3CL^pro in dose- and time-dependent manner. Bioactivity-guided fractionation and purification revealed that three flavonoids in the bioactive fractions (10–17.5 min) of AGE, including dihydromyricetin, isodihydromyricetin and myricetin, were the key constituents in AGE contribute to SARS-CoV-2 3CL^pro inactivation. Among the newly identified flavonoid-type 3CL^pro inhibitors, myricetin displayed the most potent SARS-CoV-2 3CL^pro inhibition activity, with the apparent IC_{50} value of 1.21 μM. Mass spectrometry-based peptide profiling demonstrated that dihydromyricetin and isodihydromyricetin could covalently bind on Cys300 of SARS-CoV-2 3CL^pro, while myricetin acted as a dual-site (Cys300 and Cys44) covalent inhibitor against this key enzyme. Collectively, this study provides a framework example for deciphering and characterizing the key active ingredients in herbal extract responsible for SARS-CoV-2 3CL^pro inactivation, while the newly identified SARS-CoV-2-3CL^pro inhibitors in AGE and their key pharmacophores for covalently binding on 3CL^pro offers new insights into the design and development of novel therapeutics for treating COVID-19 or other CoVs-related diseases.

CRediT authorship contribution statement

Xiong Yuan: Conceptualization, Methodology, Data Curation, Writing-Original Draft. **Zhu Guang-Hao:** Software, Methodology, Data curation. **Zhang Ya-Ni:** Methodology, Validation. **Hu Qing:** Methodology, Investigation. **Wang Hao-Nan:** Resources. **Yu Hao-Nan:** Methodology, Visualization, Data curation. **Qin Xiao-Ya:** Data curation. Guan Xiao-Qing**:** Software, Data curation. **Xiang Yan-Wei:** Supervision, Formal analysis. **Tang Hui:** Supervision, Conceptualization. **Ge Guang-Bo:** Supervision, Funding acquisition, Project administration, Writing-Reviewing and Editing.

Declaration of competing interest

The authors declare that they have no known competing financial interests or personal relationships that could have appeared to influence the work reported in this paper.

Appendix A. Supplementary data

Supplementary data to this article can be found online at https://doi.org/10.1016/j.ijbiomac.2021.07.167.

References

[1] J. Piret, G. Boivin, Pandemics throughout history, Front. Microbiol. 11 (2020), 631736, https://doi.org/10.3389/fmicb.2020.631736.

[2] A. Sharma, I. Ahmad Farouk, S.K. Lal, COVID-19: a review on the novel coronavirus disease evolution, transmission, detection, control and prevention, Viruses 13 (2021) 202, https://doi.org/10.3390/v13020202.

[3] P.H. Yang, X.L. Wang, COVID-19: a new challenge for human beings, Cell. Mol. Immunol. 17 (5) (2020) 555–557, https://doi.org/10.1038/s41423-020-0407-x.

[4] D.K. Tian, Y.Z. Liu, C.Y. Liang, L. Xin, X.L. Xie, D.Z. Zhang, M.G. Wan, H. Li, X. Q. Fu, H. Liu, W.Q. Cao, An update review of emerging small-molecule therapeutic options for COVID-19, Biomed. Pharmacother. 137 (2021), 111313, https://doi.org/10.1016/j.biopha.2021.111313.

[5] A. Shamsi, T. Mohammad, S. Anwar, S. Amani, M.S. Khan, F.M. Husain, M. T. Rehman, A. Islam, M.I. Hassan, Potential drug targets of SARS-CoV-2: from genomics to therapeutics, Int. J. Biol. Macromol. 177 (2021) 1–9, https://doi.org/10.1016/j.ijbiomac.2021.02.071.

[6] Q.X. Li, C.B. Kang, Progress in developing inhibitors of SARS-CoV-2 3C-like protease, Microorganisms 8 (8) (2020) 1250, https://doi.org/10.3390/microorganisms8081250.

[7] H.M. Mengist, A. Mohammed, R. Shi, T. Jin, Potency, safety, and pharmacokinetic profiles of potential inhibitors targeting SARS-CoV-2 main protease, Front. Pharmacol. 11 (2020), https://doi.org/10.3389/fphar.2020.630500.

[8] O. Abian, D. Ortega-Alarcon, A. Jimenez-Alesanco, L. Ceballos-Laita, S. Vega, H. T. Reyburn, B. Rizzuti, A. Velazquez-Campoy, Structural stability of SARS-CoV-2 3CLpro and identification of quercetin as an inhibitor by experimental screening, Int. J. Biol. Macromol. 164 (2020) 1693–1703, https://doi.org/10.1016/j.ijbiomac.2020.07.235.

[9] Y. Liu, C. Liang, L. Xin, X. Ren, L. Tian, X. Ju, H. Li, Y. Wang, Q. Zhao, H. Liu, W. Cao, X. Xie, D. Zhang, Y. Wang, Y. Jian, The development of coronavirus 3C-like protease (3CL) inhibitors from 2010 to 2020, Eur. J. Med. Chem. 206 (2020), 112711, https://doi.org/10.1016/j.ejmech.2020.112711.

[10] M. Jukic, D. Janežic, U. Bren, Ensemble docking coupled to linear interaction energy calculations for identification of coronavirus main protease (3CL) non-covalent small-molecule inhibitors, Molecules 25 (24) (2020) 5808, https://doi.org/10.3390/molecules25245808.

[11] F. Caruso, M. Singh, S. Belli, M. Berinato, M. Rossi, Interrelated mechanism by which the methide quinone celastrol, obtained from the roots of Tripterygium wilfordii, inhibits main protease 3CL pro of COVID-19 and acts as superoxide radical scavenger, Int. J. Mol. Sci. 21 (23) (2020) 9266, https://doi.org/10.3390/ijms21239266.

[12] Y. Kim, S.R. Mandadapu, W.C. Groutas, K.O. Chang, Potent inhibition of feline coronaviruses with peptidyl compounds targeting coronavirus 3C-like protease, Antivir. Res. 97 (2013) 161–168, https://doi.org/10.1016/j.antiviral.2012.11.005.

[13] J. Karges, M. Kalaj, M. Bembicky, S.M. Cohen, Re(I) tricarbonyl complexes as coordinate covalent inhibitors for the SARS-CoV-2 Main cysteine protease, Angew. Chem. Int. Ed. Engl. (2021 Feb 19), https://doi.org/10.1002/anie.202016768.

[14] F. Sutanto, M. Konstantinidou, A. Dömling, Covalent inhibitors: a rational approach to drug discovery, RSC. Med. Chem. 11 (8) (2020) 876–884, https://doi.org/10.1039/d0md00154f.

[15] L.L. Chen, S. Chen, C. Gui, J. Shen, X. Shen, H. Jiang, Discovering severe acute respiratory syndrome coronavirus 3CL protease inhibitors: virtual screening, surface plasmon resonance, and fluorescence resonance energy transfer assays, J. Biomol. Screen. 118 (8) (2006) 915–921, https://doi.org/10.1177/1087057106293295.

[16] Y. Xiong, G.H. Zhu, H.N. Wang, Q. Hu, L.L. Chen, X.Q. Guan, H.L. Li, H.Z. Chen, H. Tang, G.B. Ge, Discovery of naturally occurring inhibitors against SARS-CoV-2 3CL from Ginkgo biloba leaves via large-scale screening, Fitoterapia 152 (2021), 104909, https://doi.org/10.1016/j.fitote.2021.104909.

[17] Z. Jin, X. Du, Y. Xu, Y. Deng, M. Liu, Y. Zhao, B. Zhang, X. Li, L. Zhang, C. Peng, Y. Duan, J. Yu, L. Wang, K. Yang, F. Liu, R. Jiang, X. Yang, T. You, X. Liu, X. Yang, F. Bai, H. Liu, X. Liu, L.W. Guddat, W. Xu, G. Xiao, C. Qin, Z. Shi, H. Jiang, Z. Rao, H. Yang, Structure of M from SARS-CoV-2 and discovery of its inhibitors, Nature 582 (2020) 289–293, https://doi.org/10.1038/s41586-020-2223-y.

[18] M. Boberg, M. Vrana, A. Mehrotra, R.E. Pearce, A. Gaedigk, D.K. Bhatt, J.S. Leeder, B. Prasad, Age-dependent absolute abundance of hepatic carboxylesterases (CES1 and CES2) by LC-MS/MS proteomics: application to PBPK modeling of oseltamivir in vivo pharmacokinetics in infants, Drug Metab. Dispos. 45 (2) (2017) 216–223, https://doi.org/10.1124/dmd.116.072652.

[19] Y. Qian, E. Weerapana, A quantitative mass-spectrometry platform to monitor changes in cysteine reactivity, Methods Mol. Biol. 1491 (2017) 11–22, https://doi.org/10.1007/978-1-4939-6439-0_2.

[20] C.M. Fang, M.C. Ku, C.K. Chang, H.C. Liang, T.F. Wang, C.H. Wu, S.H. Chen, Identification of endogenous site-specific covalent binding of catechol estrogens to serum proteins in human blood, Toxicol. Sci. 148 (2) (2015) 433–442, https://doi.org/10.1093/toxsci/kfv190.

[21] J.P. Harrelson, B.D. Stamper, J.D. Chapman, D.R. Goodlett, S.D. Nelson, Covalent modification and time-dependent inhibition of human CYP2E1 by the meta-isomer of acetaminophen, Drug Metab. Dispos. 408 (8) (2012) 1460–1465, https://doi.org/10.1124/dmd.112.045492.

[22] D.W. Kneller, G. Phillips, K. Tan, A. Joachimiak, L. Coates, A. Kovalevsky, H. M. O'Neill, Room temperature X-ray crystallography reveals oxidation and reactivity of cysteine residues in SARS-CoV-2 3CL Mpro: insights for enzyme mechanism and drug design, IUCrJ. 7 (6) (2020) 1028–1035, https://doi.org/10.1107/S2052252520012634.

[23] P. Labute, The generalized Born/Volume integral implicit solvent model: estimation of the free energy of hydration using London dispersion instead of atomic surface area, J. Comput. Chem. 29 (10) (2008) 1693–1698, https://doi.org/10.1002/jcc.20933.

[24] A. Jakalian, D.B. Jack, C.I. Bayly, Fast, efficient generation of high-quality atomic charges. AM1-BCC model: II. Parameterization and validation, J. Comput. Chem. 23 (16) (2002) 1623–1641, https://doi.org/10.1002/jcc.10128.

[25] A. Alviz-Amador, R. Galindo-Murillo, R. Pineda-Alemán, H. Pérez-González, E. Rodríguez-Cavallo, R. Vivas-Reyes, D. Méndez-Cuadro, Development and benchmark to obtain AMBER parameters dataset for non-standard amino acids modified with 4-hydroxy-2-nonenal, Data. Brief. 21 (2018) 2581–2589, https://doi.org/10.1016/j.dib.2018.11.102.

[26] A.W. Sousa da Silva, W.F. Vranken, ACPYPE - AnteChamber PYthon parser interfacE, BMC. Res. Notes. 5 (2012) 367, https://doi.org/10.1186/1756-0500-5-367.

[27] D. Van Der Spoel, E. Lindahl, B. Hess, G. Groenhof, A.E. Mark, H.J. Berendsen, GROMACS: fast, flexible, and free, J. Comput. Chem. 26 (16) (2005) 1701–1718, https://doi.org/10.1002/jcc.20291.

[28] A. Pagoni, A. Grabowiecka, W. Tabor, A. Mucha, S. Vassiliou, L. Berlicki, Covalent inhibition of bacterial urease by bifunctional catechol-based phosphonates and phosphinates, J. Med. Chem. 64 (1) (2021), https://doi.org/10.1021/acs.jmedchem.0c01143.

[29] S. Bittner, When quinones meet amino acids: chemical, physical and biological consequences, Amino Acids 30 (3) (2006) 205–224, https://doi.org/10.1007/s00726-005-0298-2.

[30] C.M. Li, X. Teng, Y.F. Qi, B. Tang, H.L. Shi, X.M. Ma, L.H. Lai, Conformational flexibility of a short loop near the active site of the SARS-3CLpro is essential to maintain catalytic activity, Sci. Rep. 6 (2016) 20918, https://doi.org/10.1038/srep20918.

[31] J. Shi, J. Sivaraman, J. Song, Mechanism for controlling the dimer-monomer switch and coupling dimerization to catalysis of the severe acute respiratory syndrome coronavirus 3C-like protease, J. Virol. 829 (9) (2008) 4620–4629, https://doi.org/10.1128/JVI.02680-07.

[32] B. Goyal, D. Goyal, Targeting the dimerization of the Main protease of coronaviruses: a potential broad-Spectrum therapeutic strategy, ACS Comb. Sci. 22 (6) (2020) 297–305, https://doi.org/10.1021/acscombsci.0c00058.

[33] T. Muramatsu, C. Takemoto, Y.T. Kim, H. Wang, W. Nishii, T. Terada, M. Shirouzu, S. Yokoyama, SARS-CoV 3CL protease cleaves its C-terminal autoprocessing site by novel subsite cooperativity, Proc. Natl. Acad. Sci. U. S. A. 113 (46) (2016) 12997–13002, https://doi.org/10.1073/pnas.1601327113.

[34] N. Verma, J.A. Henderson, J. Shen, Proton-coupled conformational activation of SARS coronavirus Main proteases and opportunity for designing small-molecule broad-Spectrum targeted covalent inhibitors, J. Am. Chem. Soc. 142 (52) (2020) 21883–21890, https://doi.org/10.1021/jacs.0c10770.

[35] L. Zhang, D. Lin, X. Sun, U. Curth, C. Drosten, L. Sauerhering, S. Becker, K. Rox, R. Hilgenfeld, Crystal structure of SARS-CoV-2 main protease provides a basis for design of improved a-ketoamide inhibitors, Science 368 (2020) 409–412, https://doi.org/10.1126/science.abb3405.

[36] R.C.V. Carneiro, L.Y. Ye, N. Baek, G.H.A. Teixeira, S.F. O'Keefe, Vine tea (Ampelopsis grossedentata): a review of chemical composition, functional properties, and potential food applications, J. Funct. Foods 76 (2021), 104317, https://doi.org/10.1016/j.jff.2020.104317.

[37] J. Zhao, J.W. Deng, Y.W. Chen, S.P. Li, Advanced phytochemical analysis of herbal tea in China, J. Chromatography. A. 1313 (2013) 2–23, https://doi.org/10.1016/j.chroma.2013.07.039.

[38] K. Xie, X. He, K. Chen, J. Chen, K. Sakao, D.X. Hou, Antioxidant properties of a traditional vine tea, Ampelopsis grossedentata, Antioxidants 8 (8) (2019) 295, https://doi.org/10.3390/antiox8080295.

[39] J. Xiang, Q. Lv, F. Yi, Y. Song, L. Le, B. Jiang, L. Xu, P. Xiao, Dietary supplementation of vine tea ameliorates glucose and lipid metabolic disorder via akt signaling pathway in diabetic rats, Molecules 24 (10) (2019) 1866, https://doi.org/10.3390/molecules24101866.

[40] X. Song, L. Tan, M. Wang, C. Ren, C. Guo, B. Yang, Y. Ren, Z. Cao, Y. Li, J. Pei, Myricetin: a review of the most recent research, Biomed. Pharmacother. 134 (2021), 111017, https://doi.org/10.1016/j.biopha.2020.111017.

[41] S. Chen, K. Lv, A. Sharda, J. Deng, W. Zeng, C. Zhang, Q. Hu, P. Jin, G. Yao, X. Xu, Z. Ming, C. Fang, Anti-thrombotic effects mediated by dihydromyricetin involve both platelet inhibition and endothelial protection, Pharmacol. Res. 167 (2021), 105540, https://doi.org/10.1016/j.phrs.2021.105540.

[42] A. Liskova, M. Samec, L. Koklesova, S.M. Samuel, K. Zhai, R.K. Al-Ishaq, M. Abotaleb, V. Nosal, K. Kajo, M. Ashrafizadeh, A. Zarrabi, A. Brockmueller, M. Shakibaei, P. Sabaka, I. Mozos, D. Ullrich, R. Prosecky, G. La Rocca, M. Caprnda, D. Büsselberg, L. Rodrigo, P. Kruzliak, P. Kubatka, Flavonoids against the SARS-CoV-2 induced inflammatory storm, Biomed. Pharmacother. 138 (2021), 111430, https://doi.org/10.1016/j.biopha.2021.111430.

[43] H.X. Su, S. Yao, W.F. Zhao, M.J. Li, J. Liu, W.J. Shang, H. Xie, C.Q. Ke, H.C. Hu, M. N. Gao, K.Q. Yu, H. Liu, J.S. Shen, W. Tang, L.K. Zhang, G.F. Xiao, L. Ni, D. W. Wang, J.P. Zuo, H.L. Jiang, F. Bai, Y. Wu, Y. Ye, Y.C. Xu, Anti-SARS-CoV-2 activities in vitro of shuanghuanglian preparations and bioactive ingredients, Acta Pharmacol. Sin. 41 (9) (2020) 1167–1177, https://doi.org/10.1038/s41401-020-0483-6.

[44] Z. Wang, L. Yang, Chinese herbal medicine: fighting SARS-CoV-2 infection on all fronts, J. Ethnopharmacol. 270 (2021), 113869, https://doi.org/10.1016/j.jep.2021.113869.

[45] Y. Lv, S. Wang, P. Liang, Y. Wang, X. Zhang, Q. Jia, J. Fu, S. Han, L. He, Screening and evaluation of anti-SARS-CoV-2 components from Ephedra sinica by ACE2/CMC-HPLC-IT-TOF-MS approach, Anal. Bioanal. Chem. (2021) 1–10, https://doi.org/10.1007/s00216-021-03233-7.

[46] M.S. Yu, J. Lee, J.M. Lee, Y. Kim, Y.W. Chin, J.G. Jee, Y.S. Keum, Y.J. Jeong, Identification of myricetin and scutellarein as novel chemical inhibitors of the SARS coronavirus helicase, nsP13, Bioorg. Med. Chem. Lett. 22 (2012) 4049–4054, https://doi.org/10.1016/j.bmcl.2012.04.081.

[47] T.T. Nguyen, H.J. Woo, H.K. Kang, V.D. Nguyen, Y.M. Kim, D.W. Kim, S.A. Ahn, Y. Xia, D. Kim, Flavonoid-mediated inhibition of SARS coronavirus 3C-like protease expressed in Pichia pastoris, Biotechnol. Lett. 34 (5) (2012) 831–838, https://doi.org/10.1007/s10529-011-0845-8.

[48] C.G. Fraga, K.D. Croft, D.O. Kennedy, F.A. Tomás-Barberán, The effects of polyphenols and other bioactives on human health, Food Funct. 10 (2) (2019, 2019) 514–528, https://doi.org/10.1039/c8fo01997e.

[49] X.X. Wang, X. Lv, S.Y. Li, J. Hou, J. Ning, J.Y. Wang, Y.F. Cao, G.B. Ge, B. Guo, L. Yang, Identification and characterization of naturally occurring inhibitors against UDP-glucuronosyltransferase 1A1 in fructus psoraleae (Bu-gu-zhi), Toxicol. Appl. Pharmacol. 289 (1) (2015) 70–80, https://doi.org/10.1016/j.taap.2015.09.003.

[50] X. Lv, J.B. Zhang, X.X. Wang, W.Z. Hu, Y.S. Shi, S.W. Liu, D.C. Hao, W.D. Zhang, G. B. Ge, J. Hou, L. Yang, Amentoflavone is a potent broad-spectrum inhibitor of human UDP-glucuronosyltransferases, Chem. Biol. Interact. 284 (2018) 48–55, https://doi.org/10.1016/j.cbi.2018.02.009.

[51] H. Xin, X.Y. Qi, J.J. Wu, X.X. Wang, Y. Li, J.Y. Hong, W. He, W. Xu, G.B. Ge, L. Yang, Assessment of the inhibition potential of licochalcone a against human UDP-glucuronosyltransferases, Food Chem. Toxicol. 90 (2016) 112–122, https://doi.org/10.1016/j.fct.2016.02.007.